ROYAL SOCIETY
OF CHEMISTRY

PAPER

Check for updates

Stoichiometric anion exchange by a low-dielectric-constant solvent for highly-doped conjugated polymers with enhanced environmental stability†

Daegun Kim,‡[a] Jiwoo Min,‡[b] Kyeong-Jun Jeong,‡[c] Eunsol Ok,[b] Jaemin Im,[d] Hyun Ho Choi,[d] Giwon Lee, [iD] [e] Chang Yun Son [iD] *[c] and Kilwon Cho [iD] *[b]

High-degree doping of conjugated polymers often employs a strong redox agent, which facilitates polymer ionization but results in poor environmental stability for the counter-ion. Here, we demonstrate an anion-exchange doping using a model study that systematically investigates the effect of the solvent dielectric constant on both doping and anion exchange. The dielectric constant significantly affects the initial doping of poly(2,5-bis(3-hexadecylthiophene-2-yl)thieno[3,2-*b*]thiophene) (**PBTTT**) films using $FeCl_3$, as well as in the subsequent anion exchange of $[FeCl_4]^-$ to dodecylbenzenesulfonate ($[DBS]^-$). A solvent with a higher dielectric constant improves the $FeCl_3$ doping efficiency but hinders the subsequent anion exchange. Such conflicting effects can be resolved by stepwise immersion in separate solutions of $FeCl_3$ and dodecylbenzenesulfonic acid (**DBSA**). Stepwise anion-exchange doping achieves high electrical conductivity with improved environmental stability, while also allowing for the application of desired anions that require extended time for the direct doping method, such as in Brønsted acid doping.

1. Introduction

Conducting polymers (CPs) are promising candidates as active materials or electrodes for flexible electronics, offering advantages such as low processing costs and good mechanical flexibility.[1,2] However, as-synthesized CPs often exhibit low carrier densities (n) and low carrier mobilities (μ), both of which cause very low electrical conductivities (σ).[3] Doping CPs can increase n, thereby enhancing σ.[4–7] Doping of CPs typically exploits a redox reaction to generate charge carriers in CPs *via* charge transfer with small dopant molecules.[5,8,9] For efficient doping of CPs, the dopant should have a high redox potential for oxidation (p-type) or reduction (n-type) of CPs[4,10,11] and a sufficiently small size for facile incorporation in CPs.[12–14] For example, polyacetylene exhibited an excellent $\sigma \sim 10^5$ S cm^{-1} by iodine doping, for which the Nobel prize in chemistry was granted in 2000.[15] However, such a small size of atomic dopant resulted in

poor environmental stability of the counter-ion which is readily degraded in the CP film by various environmental factors: heat or reaction with oxygen or water molecules.[16] Hence, molecular dopants, such as $FeCl_3$,[17,18] 2,3,5,6-tetrafluoro-tetracyanoquino-dimethane (F4TCNQ),[14,19,20] and tetramethylhydroquinone (TMQH),[21] have been developed to induce a stable and high-degree doping of CPs. Nonetheless, the sizes of such molecular dopants are made to be sufficiently small, representing the trade-off between doping efficiency (diffusion into CPs) and environmental stability (degradation in CPs).[12]

Recently, H. Sirringhaus and coworkers reported a high degree of doping in CPs using ion-exchange doping, in which the counter-ions formed by the redox reaction of the dopant molecules were subsequently replaced by anions from an added ionic liquid.[22,23] It was claimed that the redox potential of the dopant molecule serves as the driving force for anion exchange in a manner analogous to the applied electrical potential in electrochemical doping. Doping of CPs with simultaneous counter-ion exchange offers insight into how the trade-off between doping efficiency and environmental stability when using a single dopant molecule can be resolved. However, the reported ion-exchange doping methods homogeneously added molecular dopants and ionic liquids using the same solvent, necessitating the use of a highly polar solvent that dissolves the molecular dopants and stabilizes their redox reactions.[5,17,24–26] The polar solvent also limits the choice of replaceable ions, as the solubility in the polar solvent requires an ionic salt to have high polarity. An effective counter-ion should have a wide electrochemical window to prevent charge transfer from the

[a]School of Chemical, Biological and Battery Engineering, Gachon University, Seongnam 13120, Korea

[b]Department of Chemical Engineering, Pohang University of Science and Technology, Pohang 37673, Korea. E-mail: kwcho@postech.ac.kr

[c]Department of Chemistry, Seoul National University, Seoul 08826, Korea. E-mail: changyunson@snu.ac.kr

[d]Department of Materials Engineering and Convergence Technology, Gyeongsang National University, Jinju 52828, Korea

[e]Department of Chemical Engineering, Kwangwoon University, Seoul 01899, Korea

† Electronic supplementary information (ESI) available. See DOI: https://doi.org/10.1039/d5ta01703c

‡ These authors contributed equally to this work.

counter-ion back to CPs, good miscibility with CPs,[22] and a sufficiently large size for environmental stability.[27] To meet all these requirements in a single counter-ion, the counter-ion should possess not only an electrochemically stable ionic functional group but also a considerably large hydrocarbon, which results in poor solubility in polar solvents.[28] However, using a solvent with a low dielectric constant to dissolve such ions provides insufficient stabilization for the charged species after the redox reaction, thus suppressing the carrier density increment upon doping of CPs.[22,29] The mismatch of the required solvent dielectric constant for the dopant and the counter-ion cannot be resolved in homogeneous doping.

In this work, ion-exchange doping was conducted through a two-step process using two separate solutions for the redox reaction and the ion exchange, respectively. By separating the redox reaction and the ion exchange, different solvents can be adopted for each process. To systematically study the optimal solvent conditions for these processes, solvents with varied dielectric constants were employed to investigate the effect of solvent on the environment around the charge carriers and anions during the anion-replacement step in a model system. Dodecylbenzenesulfonic acid (**DBSA**) was selected for the model study, as the ionized dodecylbenzenesulfonate ([DBS]$^-$) is a decent counter-ion exhibiting good miscibility in solvents with a wide range of dielectric constants. **DBSA** can also directly oxidize CPs *via* Brønsted-acid doping, allowing for an evident comparison between stepwise ion-exchange doping and direct doping. Poly(2,5-bis(3-hexadecylthiophen-2-yl)thieno[3,2-*b*]thiophene) (**PBTTT**) films were initially doped using FeCl$_3$ and subsequently immersed in **DBSA** diluted in solvents with varying dielectric constants. Quantitative evaluation of carrier densities and computational calculations on the binding state between the CP and counter-ion revealed that a partially polar solvent was favored for the redox reaction, whereas a non-polar solvent was favored for Brønsted-acid doping and anion exchange. With suitable solvents, the stepwise ion-exchange doping not only facilitated the incorporation of bulky and non-polar counter-ions into CPs but also achieved electrical conductivity comparable to that obtained by conventional direct doping.
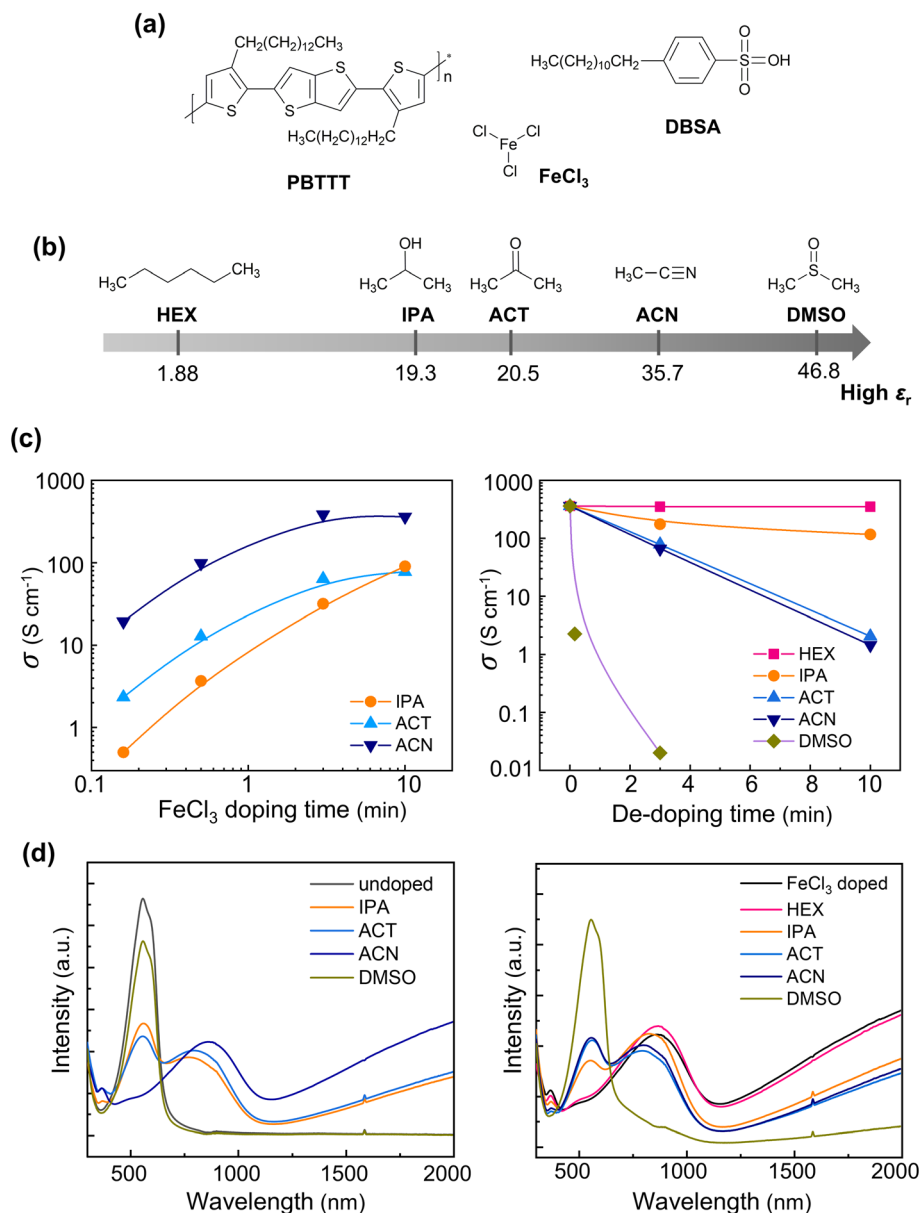
2. Results and discussion

The solvent effect during anion exchange was systematically investigated in a model system, where **PBTTT** film was first doped by FeCl$_3$, and then the [FeCl$_4$]$^-$ anion was sequentially exchanged for the [DBS]$^-$ anion under various solvent conditions. **PBTTT** is a solution-processable conjugated polymer widely used in semiconducting devices, such as field-effect transistors, chemical sensors and thermoelectric generators, because of its high carrier mobility[30–33] (Fig. 1a). The electrical conductivity of **PBTTT** can be readily enhanced when the polymer backbone is charged through a redox reaction with an added dopant. **PBTTT** is typically oxidized to achieve p-type character by either solution-mixing or sequential doping with strong oxidants. FeCl$_3$ is a commonly used oxidant for p-type doping as it forms a relatively stable CP-anion pair. **DBSA** is

a strong Brønsted acid that protonates polymer or organic solvent, leaving the [DBS]$^-$ anion. The benzene ring in the [DBS]$^-$ anion donates electrons, so the [DBS]$^-$ anion can experience significant stabilization when paired with a positive polaron. Therefore, competition between [DBS]$^-$ and [FeCl$_4$]$^-$ anions as counter-ions is expected when **DBSA** is sequentially applied to FeCl$_3$-doped **PBTTT** film. **DBSA** is also soluble in both polar and non-polar solvents due to the coexistence of a polar sulfonic acid group and a long alkyl chain.[34] Hence, **DBSA** is suitable for use in the model study to evaluate the effect of various solvents across a wide range of dielectric constants (Fig. 1b).

To evaluate the ion-exchange behavior, **PBTTT** films were first doped by immersing spin-coated **PBTTT** films into an FeCl$_3$ solution for the desired time. The polar FeCl$_3$ can only be dissolved in polar solvents. FeCl$_3$ doping induced higher electrical conductivity in **PBTTT** films with acetonitrile (**ACN**) compared to isopropanol (**IPA**) or acetone (**ACT**) (Fig. 1c). The electrical conductivity of **PBTTT** films barely exceeded 0.1 S cm^{-1} when the FeCl$_3$ solution was prepared with dimethyl sulfoxide (**DMSO**), which has the highest dielectric constant among the solvents used in this study. **PBTTT** films doped by FeCl$_3$ in **ACN** were then immersed in pure solvents to assess the stability of the [FeCl$_4$]$^-$ anion. The electrical conductivity of the **PBTTT** films dramatically decreased with increasing dielectric constant of the solvent. The UV-vis-NIR absorption spectra of the **PBTTT** films supported the electrical measurements (Fig. 1d). The pristine **PBTTT** film exhibited a notable absorption at 560 nm. Upon doping, this absorption decreased while new absorptions appeared at 800 nm and broadly at wavelengths over 1200 nm. These absorptions correspond to the neutral **PBTTT** chain, charged **PBTTT** chain, and generated polaron, respectively.[35] Doping with FeCl$_3$ in **ACN**, which produced the highest electrical conductivity among the solvents used, almost completely suppressed the absorption of the neutral **PBTTT** chain and resulted in the strongest absorptions for the charged **PBTTT** chain and polarons, compared to the other solvents. This result was consistent with the electrical conductivity results. Rinsing the doped **PBTTT** films with solvents led to the opposite effect in the UV-vis-NIR spectra. Rinsing with polar solvents, such as **IPA**, **ACT**, **ACN**, and **DMSO** caused decreases in the absorptions associated with the charged **PBTTT** chain and polarons, while increasing the absorption of the neutral **PBTTT** chain. On the other hand, rinsing with the non-polar solvent hexane (**HEX**) did not cause significant changes in either the electrical conductivity or the UV-vis-NIR absorption spectrum of the FeCl$_3$-doped **PBTTT** film.

The effect of the dielectric constant on doping efficiency is primarily related to the stabilization of the oxidized **PBTTT**-anion pair and the swelling of the **PBTTT** film during sequential doping.[29] A solvent with a higher dielectric constant can enhance doping by stabilizing ion species, including oxidized **PBTTT** and ionized dopant molecules, while a solvent with a lower dielectric constant can cause significant swelling of the **PBTTT** film, promoting the diffusion of dopant molecules. Hence, the dielectric constant should be carefully selected for a specific dopant-CP system. **PBTTT** films were not effectively
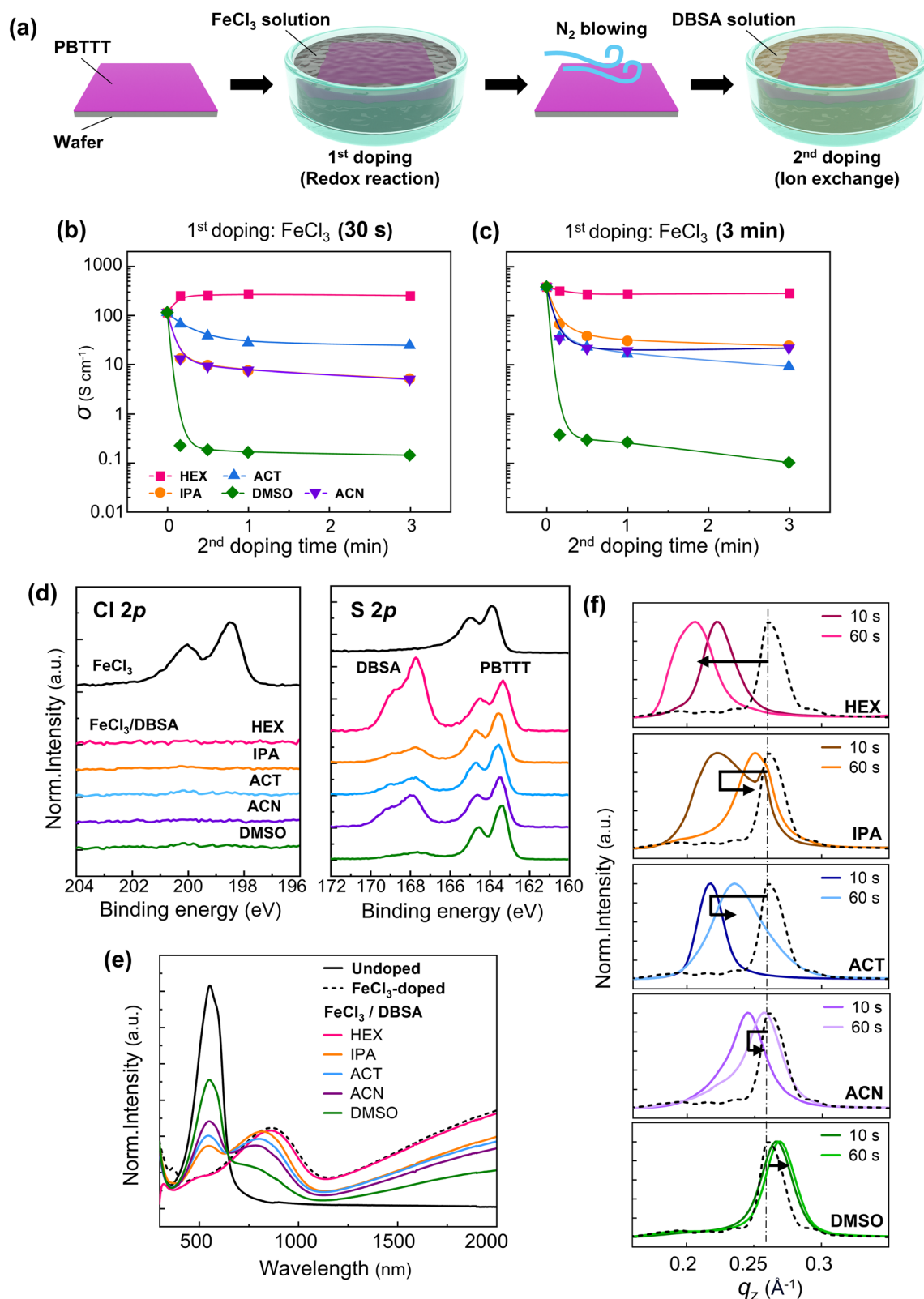
This journal is © The Royal Society of Chemistry 2025

J. Mater. Chem. A, 2025, **13**, 18966–18977 | **18967**

Fig. 1 (a) Chemical structures of PBTTT, FeCl$_3$, and DBSA. (b) Chemical structures of solvents with different dielectric constants ε_r. (c) The electrical conductivity σ and (d) the UV-vis-NIR spectra of PBTTT films after FeCl$_3$ doping with various solvents (left) and FeCl$_3$-doped PBTTT films rinsed (dedoped) with various solvents (right).

doped by FeCl$_3$ in **DMSO**, which has a higher dielectric constant than the other solvents. The poor doping efficiency in **DMSO** was attributed to the poor solubilization of **PBTTT** in **DMSO**, which exhibited a higher contact angle on the **PBTTT** surface compared to the other solvents (Fig. S1†). The strong coordinating ability of **DMSO** may also contribute to the low electrical conductivity, as it can reduce the oxidizing power of FeCl$_3$. On the other hand, dedoping of the doped **PBTTT** films through solvent rinsing became progressively stronger when a solvent with a higher dielectric constant was used. This result indicates that the [FeCl$_4$]$^-$ anion is unstable and readily loses coulombic interaction with the [**PBTTT**]$^+$ chain in polar environments. Such poor stability of the counter-ion in polar environments is

common for various molecular dopants due to their strong polarity indices and small sizes.[36] Therefore, the counter-ion should be replaced with an ion with low polarity and large size to improve the stability of the doped state in the **PBTTT** film.

The **PBTTT** film was first doped with FeCl$_3$, which triggered the redox reaction with **PBTTT**. The FeCl$_3$-doped **PBTTT** film was then immersed in a **DBSA** solution for a desired duration to induce anion exchange between the unstable [FeCl$_4$]$^-$ anion and the [DBS]$^-$ anion (Fig. 2a). The electrical conductivity of the **PBTTT** film was around 100 S cm^{-1} after doping with FeCl$_3$ in **ACN** for 30 s, during which only a small portion of the **PBTTT** repeat units was oxidized, resulting in a relatively low charge

18968 | J. Mater. Chem. A, 2025, **13**, 18966–18977

This journal is © The Royal Society of Chemistry 2025

Fig. 2 (a) Schematic process of sequential ion-exchange doping. The σ values of **PBTTT** films after doping of $FeCl_3$ (**ACN**) for (b) 30 s or (c) 3 min followed by the **DBSA** treatment in various solvents. (d) XPS Cl 2p and S 2p spectra, (e) UV-vis-NIR absorption spectra, and (f) GIWAXS patterns along the q_z direction of $FeCl_3$-doped (dotted) and $FeCl_3$/**DBSA**-doped (solid, color) **PBTTT** films. $FeCl_3$ was doped with CAN for 3 min. The **DBSA** solution for the anion exchange was prepared with the labelled solvent. The **DBSA** treatment time was 1 min, unless it is specified (10 s or 60 s).

This journal is © The Royal Society of Chemistry 2025

J. Mater. Chem. A, 2025, **13**, 18966–18977 | **18969**

carrier density. The resulting electrical conductivity after doping would be primarily determined by the doping efficiency, as the **PBTTT** morphology did not vary significantly depending on the solvent (Fig. S2†). The sequential ion exchange following 30 s of FeCl$_3$ doping was significantly affected by the solvent choice (Fig. 2b). When immersed in a **DBSA** solution with polar solvents, the FeCl$_3$-doped **PBTTT** film exhibited a substantial decrease in electrical conductivity, with the decrement being larger for solvents with a higher dielectric constant. Conversely, the electrical conductivity of the FeCl$_3$-doped **PBTTT** film increased following **DBSA** treatment in **HEX**. An increase in electrical conductivity upon **DBSA** treatment indicated additional doping by **DBSA**, which presumably generates charge carriers through protonation of the **PBTTT** chain.[37,38] The results confirmed that the dielectric constant was a primary property affecting both doping and the anion exchange process, though the electrical conductivity after **DBSA** treatment was not completely proportional to the dielectric constants of the solvents used. This minor inconsistency was possibly attributed to solvent properties such as pK_a, catalytic effect, and stabilization of protonation, all of which are related to direct doping by **DBSA**. The direct doping by **DBSA** will be examined in the final section. Similar results were obtained for **DBSA** treatment on highly doped **PBTTT** films, which had undergone FeCl$_3$ doping for 3 min (Fig. 2c). The electrical conductivity of the highly doped **PBTTT** film decreased from 350 S cm^{-1} to below 10 S cm^{-1} after **DBSA** treatment in polar solvents, whereas only a slight decrease in the electrical conductivity was observed for **DBSA** treatment in **HEX**. The results of the **DBSA** treatment were analogous to those of solvent rinsing, where polar solvents significantly removed polarons and ionized dopants from the **PBTTT** film, while the non-polar solvent did not.

The anion exchange between the [FeCl$_4$]$^-$ and [DBS]$^-$ anions was further investigated using X-ray photoelectron spectroscopy (XPS) (Fig. 2d). The as-doped **PBTTT** film exhibited notable Cl 2p peaks originating from [FeCl$_4$]$^-$ anions. Two distinguishable peaks were attributed to spin–orbit splitting. When the FeCl$_3$-doped **PBTTT** film underwent anion exchange by **DBSA** treatment, the Cl 2p peaks disappeared regardless of the solvent used, indicating that **DBSA** treatment completely removed the [FeCl$_4$]$^-$ anions from the **PBTTT** film by inducing anion exchange or by annihilating polarons (Fig. S3†). On the other hand, **DBSA** treatment generated new peaks in the S 2p spectra. The as-doped **PBTTT** film exhibited two distinct S 2p peaks at binding energies between 162 and 166 eV, which arose from the S atoms in the thiophene and thienothiophene rings in the **PBTTT** chain.[22] The chemical environments around S atoms in the thiophene and thienothiophene are very similar, so their S 2p peaks are hardly distinguishable. The existence of two peaks were again attributed to spin–orbit splitting.[39] Anion exchange by **DBSA** yielded new S 2p peaks at binding energies between 167 and 170 eV, which originated from the sulfonate group in the [DBS]$^-$ anions.[40] These peaks were more intense when a non-polar solvent was used compared to a polar solvent. Considering the electrical conductivities after **DBSA** treatment, the XPS results provided direct evidence that the [DBS]$^-$ anions replaced the [FeCl$_4$]$^-$ anions to stabilize oxidized **PBTTT** chains.

The XPS results also suggested that polar solvents washed away the [FeCl$_4$]$^-$ anions and reduced the oxidation level of the **PBTTT** chain, rather than inducing a stoichiometric replacement of the [FeCl$_4$]$^-$ anions with the [DBS]$^-$ anions.

The UV-vis-NIR absorption spectra also confirmed that **DBSA** treatment in a polar solvent decreased the oxidation level of the **PBTTT** chain (Fig. 2e). As observed during pure solvent rinsing, the use of a polar solvent for **DBSA** treatment caused a significant increase in absorption by the neutral **PBTTT** chain at 560 nm, along with decreases in absorption by the oxidized **PBTTT** chain at 800 nm and broad absorption by polarons at wavelengths over 1200 nm. The reduction in the oxidation level of the **PBTTT** chain by anion exchange was greater when a solvent with a higher dielectric constant was used. On the other hand, the content of the [DBS]$^-$ anions in **PBTTT** films showed a relatively weak correlation with the dielectric constant of the solvent used for **DBSA** treatment. For example, according to the XPS spectra (Fig. 2d, right), a higher [DBS]$^-$ content was expected for **ACN** compared to **IPA** or **ACT**, both of which have lower dielectric constants than **ACN**. The mismatch between XPS and UV-vis-NIR spectra suggested that physically adsorbed **DBSA** in polar circumstances did not fully dissociate to form [DBS]$^-$ anions that could replace [FeCl$_4$]$^-$ anions.

The incorporation of the [DBS]$^-$ anion in the crystalline **PBTTT** domain was investigated using grazing-incidence wide-angle X-ray scattering (GIWAXS) (Fig. 2f and S4†). The GIWAXS patterns of undoped and doped **PBTTT** films showed several (h00) peaks that represent the lamellar spacing (d spacing) between **PBTTT** lamellae along the out-of-plane direction. FeCl$_3$ doping shifted the (100) peak to a lower q value, indicating an increase in the d spacing as a result of incorporating [FeCl$_4$]$^-$ anions between the **PBTTT** lamellae. FeCl$_3$ doping increased the d spacing from 20.9 to 24.1 Å. Anion exchange in all solvents, except for **DMSO**, shifted the (100) peak further to lower q_z values along the out-of-plane direction, indicating that **DBSA** or [DBS]$^-$ anions were incorporated between **PBTTT** lamellae, thus expanding the d spacing. When **DMSO** was used as the solvent for **DBSA** treatment, it effectively washed away the incorporated [FeCl$_4$]$^-$ anions instead of replacing them with [DBS]$^-$ anions, causing the expanded **PBTTT** lamellar structure to shrink back, resulting in a shift of the (100) peak to higher q_z values. The degree of lamellar expansion in FeCl$_3$-doped **PBTTT** films by anion exchange depended on the solvent and the immersion duration. **DBSA** treatment with **HEX** as the solvent (**DBSA/HEX** treatment) increased the d spacing from 24.1 to 27.6 Å after 10 s of immersion. The d spacing was further increased with a longer immersion time of 60 s. In contrast, **DBSA/IPA**, **DBSA/ACT**, and **DBSA/ACN** treatments increased the d spacing after 10 s of immersion, but the d spacing decreased with longer immersion of 60 s.

Note that the lamellar expansion after 10 s of **DBSA** treatment monotonically decreased with increasing dielectric constant. The lamellar expansion upon **DBSA** treatment indicated the incorporation of **DBSA** or [DBS]$^-$ ions between the **PBTTT** lamellae. Considering the short immersion time, the diffusion of **DBSA** into the **PBTTT** film would predominantly

affect the lamellar expansion, rather than the anion exchange rate. Therefore, the lamellar expansion by the **DBSA** treatment for 10 s would increase with greater miscibility with **PBTTT**, whose long alkyl chain interacts strongly with solvents of low dielectric constants. With extended **DBSA** treatment, the lamellar expansion by **DBSA** incorporation increased in non-polar environments, whereas the use of a polar solvent led to lamellar shrinkage.

The observed lamellar shrinkage in polar environments indicated that a significant portion of the **DBSA** intercalated with the **PBTTT** film diffused out without undergoing anion exchange. The diffusion of **DBSA** in and out of the **PBTTT** film may have originated from the rapid escape of the $[FeCl_4]^-$ anion, whose redox potential acted as a driving force to promote **DBSA** diffusion into the **PBTTT** film.[22] When the **DBSA** solution first contacts the **PBTTT** surface, **DBSA** diffuses into the **PBTTT** film due to the strong electrochemical potential exerted by the embedded $[FeCl_4]^-$ anions. Non-polar solvents did not dissolve the $[FeCl_4]^-$ anion, which led to continued diffusion of **DBSA** and an increased probability of anion exchange with increasing treatment time. In contrast, polar solvents caused the $[FeCl_4]^-$ anions to escape quickly from the **PBTTT** film, reducing both the driving force for **DBSA** diffusion and the probability of anion exchange over treatment time. The **DBSA** treatment using **ACT** as the solvent exhibited relatively small lamellar shrinkage after 60 s of treatment, possibly due to the stabilization of **DBSA** within the **PBTTT** film *via* hydrogen bonding. Though a considerable amount of **DBSA** was expected to remain between the crystalline **PBTTT** lamellae, the decrease in electrical conductivity after the **DBSA/ACT** treatment suggested that most **DBSA** molecules were unionized.

The solvent effect on the anion exchange was further investigated through quantitative characterization of the carrier mobility and carrier density of **PBTTT** films. The carrier mobility of doped **PBTTT** films was measured using a four-point probe field-effect transistor (FET) configuration, according to our previous work[41] (Fig. 3a). Briefly, four electrodes were deposited in a line with equal spacing onto a SiO_2/Si wafer, followed by spin-coating of the **PBTTT** film and subsequent doping and anion exchange processes (Fig. 3b). Among the four electrodes, the outer two served as the source and drain, where the drain voltage V_{SD} was applied, while the inner two acted as probes to measure the voltage drop V_{4p}, thereby excluding the voltage drops caused by Schottky-barrier contact resistance from the calculation of carrier mobility. The FET mobility μ_{2p} in the conventional source-drain (two-point probe) configuration is given by the following equation:

$$\mu_{2p} = \frac{1}{C_i V_{SD}} \frac{L_{2p}}{W} \frac{\partial I_{SD}}{\partial V_G}, \tag{1}$$

where C_i [F] is the gate-channel capacitance, and L_{2p} [m] and W [m] are the length and width of the channel, respectively. I_{SD} [A] is the drain current and V_G is the gate voltage. On the other hand, the equation for the FET mobility in the four-point probe configuration includes a slight modification:

$$\mu_{4p} = \frac{\alpha}{C_i} \frac{L_{4p}}{W} \frac{\partial I_{SD}/V_{4p}}{\partial V_G}, \tag{2}$$

where L_{4p} [m] is the distance between the inner electrodes among four electrodes. $\alpha = (1 - t/D)^{-1}$ is a correction factor, where $t = 10$ μm and $D = 300$ μm are the width of the electrode and the spacing between inner electrodes. α was proven to effectively correct the longitudinal channel shunting effect in our previous work.[41] Notice that I_{SD}/V_{4p} is just a resistance between inner electrodes. Hence, the conductivity σ_{4p} is given by $\sigma_{4p} = \frac{L_{4p}}{Wt} \frac{I_{SD}}{V_{4p}}$, where t is t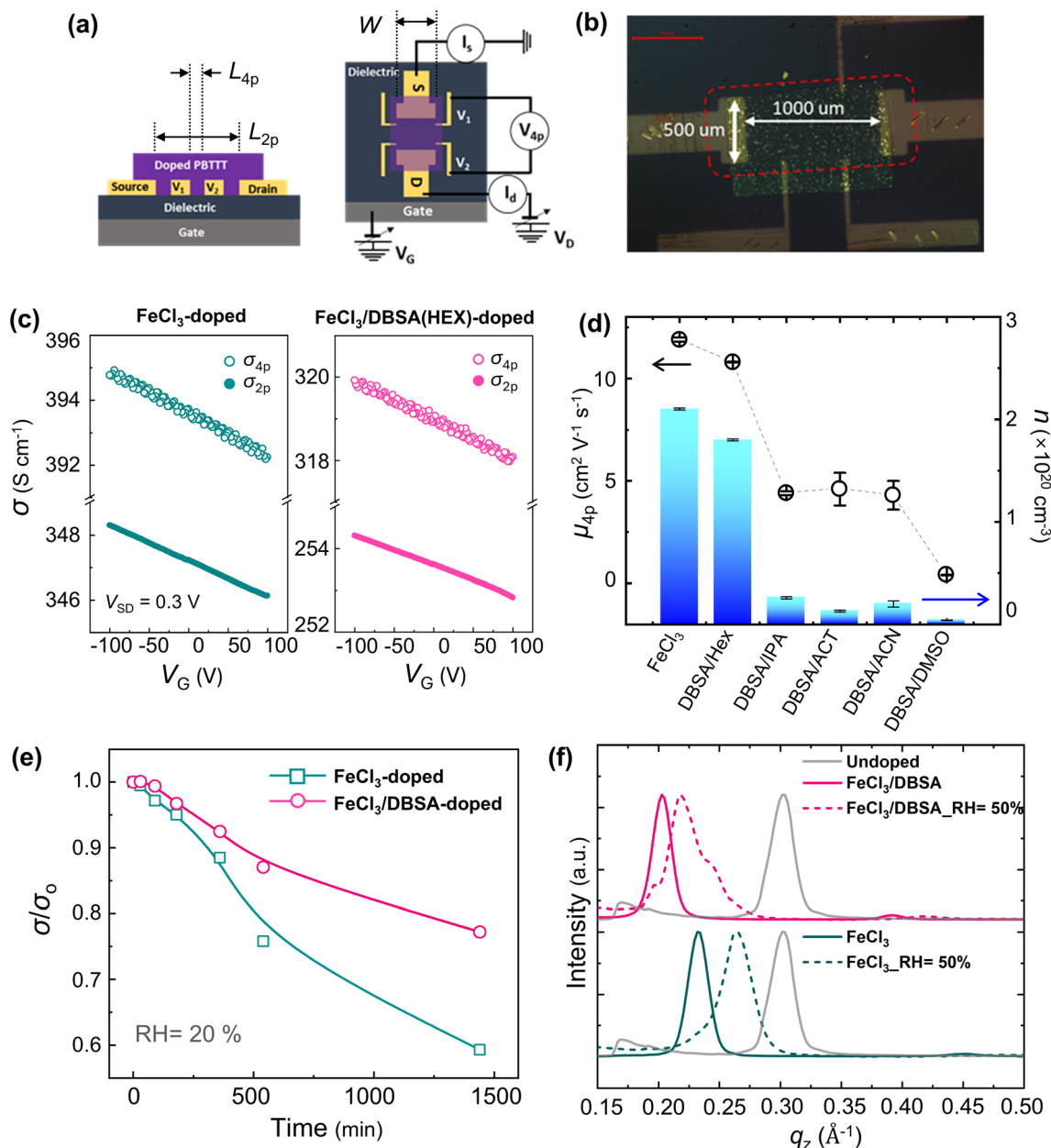he thickness of the **PBTTT** film. This equation is identical to that used in a conventional four-point probe measurement to determine conductivity. The doped **PBTTT** film had a very high carrier density, which showed a noticeable linear correlation with the applied V_G in the range between -100 and $+100$ V, despite a small change induced by the field effect. The electrical conductivity of the **PBTTT** film was measured using both two- and four-point probe methods with respect to V_G. The conductivity σ_{2p} in the two-probe configuration is given by $\sigma_{2p} = \frac{L_{2p}}{Wt} \frac{I_{SD}}{V_{SD}}$. The value of σ_{2p} was far smaller than that of σ_{4p}, implying a considerable voltage loss due to contact resistance (Fig. 3c). Carrier mobilities were obtained from the slope of $\sigma_{2p}(\sigma_{4p})$ *vs.* V_G in the two-point probe (four-point probe) configuration as follows:

$$\mu_{2p}(\mu_{4p}) = \frac{t}{C_i} \frac{\partial \sigma_{2p}(\sigma_{4p})}{\partial V_G}, \tag{3}$$

The $FeCl_3$-doped **PBTTT** film exhibited carrier mobilities of $\mu_{2p} = 10.1 \pm 0.01$ cm^2 V^{-1} s^{-1} and $\mu_{4p} = 11.9 \pm 0.06$ cm^2 V^{-1} s^{-1}. The $FeCl_3$-doped **PBTTT** film after the **DBSA/HEX** treatment ($FeCl_3$/**DBSA**-doped **PBTTT** film) had mobilities of $\mu_{2p} = 8.4 \pm 0.03$ cm^2 V^{-1} s^{-1} and $\mu_{4p} = 10.8 \pm 0.02$ cm^2 V^{-1} s^{-1}. The difference in carrier mobilities of these **PBTTT** films was 17% and 9% by the two-point and four-point probe measurements, respectively. The enlarged difference in carrier mobilities in the two-point probe measurement originated from the underestimation of the carrier mobility at an increased contact resistance.

The carrier mobilities of **PBTTT** films were therefore obtained using the four-point probe FET measurement for explicit comparison. The carrier density n of a **PBTTT** film was calculated from the conductivity σ and μ_{4p}; *i.e.*, $n = \sigma/e\mu_{4p}$, where e is the charge of an electron. **PBTTT** film was highly-doped, so using FET mobility (μ_{4p}) would not make a significant error in estimating n. Both n and μ_{4p} of the $FeCl_3$-doped **PBTTT** film were largely maintained after the **DBSA/HEX** treatment (Fig. 3d). In contrast, the **DBSA** treatment with a polar solvent critically decreased both n and μ_{4p}. The decrease in μ_{4p} associated with dedoping was attributed to a reduction in the probability of activation, in which a charge carrier has sufficient energy to reach an extended number of accessible states. This occurred because the density of states (DOS) near the Fermi level decreased dramatically as the Fermi level shifted toward the forbidden region as a result of dedoping.[42] The decrease in both

This journal is © The Royal Society of Chemistry 2025

J. Mater. Chem. A, 2025, **13**, 18966–18977 | **18971**

Fig. 3 (a) and (b) The device structure for four-point probe FET measurement where $L_{2p} = 1000$ μm, $L_{4p} = 500$ μm and $W = 500$ μm. (c) Obtained σ values of FeCl$_3$-doped (left) and FeCl$_3$/DBSA-doped (right) PBTTT films by performing two-point and four-point probe FET measurement. (d) The carrier mobility μ_{4p} obtained in four-point probe FET (column) and the carrier density n (line) of FeCl$_3$-doped and FeCl$_3$/DBSA-doped PBTTT films. (e) Changes in σ of FeCl$_3$-doped and FeCl$_3$/DBSA-doped PBTTT films at room temperature with relative humidity (RH) of 20%. (f) (100) peaks along the out of plane direction of FeCl$_3$-doped and FeCl$_3$/DBSA-doped PBTTT films with and without exposure to humid conditions (RH = 50%) for 1 h. FeCl$_3$ was doped with ACN for 3 min. The DBSA was applied with HEX as the solvent unless it is specified.

n and μ_{4p} upon DBSA treatment in polar environments underscored the importance of solvent selection in anion exchange processes.

With the proper choice of solvent for each doping and anion exchange step, the FeCl$_3$/DBSA-doped film showed improved environmental stability compared to the FeCl$_3$-doped PBTTT film (Fig. 3e). The electrical conductivities of FeCl$_3$- and FeCl$_3$/DBSA-doped PBTTT films decreased upon exposure to ambient conditions at room temperature with 20% humidity, because of polaron annihilation and counter-ion solvation by chemicals in

the ambient air. However, anion exchange from the [FeCl$_4$]$^-$ to the [DBS]$^-$ anion suppressed the decrease in electrical conductivity, reducing the change by almost half after 24 h of exposure to ambient conditions. It is noteworthy that almost 80% of electrical conductivity was preserved after 24 h exposure to ambient conditions with anion replacement, considering doped conjugated polymer films often lose significant portions of their electrical conductivity upon exposure to ambient conditions for a few hours.[43] Exposure to humid conditions with 50% humidity for 1 h shifted the (100) peaks of FeCl$_3$- and

18972 | J. Mater. Chem. A, 2025, 13, 18966–18977

This journal is © The Royal Society of Chemistry 2025

$FeCl_3$/**DBSA**-doped **PBTTT** films to higher values, indicating lamellar shrinkage caused by the escape of counter-ions from the **PBTTT** film due to solvation by water molecules (Fig. 3f). The anion exchange from the $[FeCl_4]^-$ to the $[DBS]^-$ anion also mitigated the shift of the (100) peak, suggesting that the $[DBS]^-$ anion improved the water resistance of the doped **PBTTT** film, possibly due to the bulky and non-polar alkyl chain of the $[DBS]^-$ anion.

To elucidate the mechanism of the anion exchange process, the effect of the solvent dielectric constant on the binding of anions to polarons and on the doping level was evaluated using DFT calculations. Benzenesulfonate $[BS]^-$ and C_0-BTTT were used as surrogates for the $[DBS]^-$ ion and **PBTTT**, respectively, to maintain computational tractability without significantly deviating from the real chemical environment (see Fig. S5 and S6 in ESI Section 2† for details). The energy level of the $[BTTT]^+$–$[FeCl_4]^-$ pair or the $[BTTT]^+$–$[BS]^-$ pair decreased considerably when the intermolecular distance was reduced from an infinitely large distance (separated) to an optimized distance (Fig. 4a). The energy decrement upon ion-pair formation corresponds to the binding energy, which represents the stabilization of charged species *via* coulombic interaction. A larger binding energy of the $[BTTT]^+$–$[BS]^-$ pair than that of the $[BTTT]^+$–$[FeCl_4]^-$ pair indicated that the difference in binding energy acted as the driving force of anion exchange. Notice that the binding energies of the $[BTTT]^+$–$[BS]^-$ and $[BTTT]^+$–$[FeCl_4]^-$

pairs and their difference ΔE_{ex} both diminished in **DMSO** compared to the values in **HEX**. The reduced binding energies in a polar environment can be attributed to the stabilization of charged species by the solvent. The weakening of $[BTTT]^+$–$[FeCl_4]^-$ binding in a polar environment would promote the escape of the $[FeCl_4]^-$ anion from the polaron. The dissociation of the $[FeCl_4]^-$ anion can initiate the anion exchange process, but the reduction in ΔE_{ex} in a polar solvent weakened the driving force for anion exchange, thereby requiring a longer time in a polar solvent compared to a non-polar solvent. As a result, in a polar solvent, the $[FeCl_4]^-$ anion would quickly dissociate from the polaron prior to the completion of anion exchange.

The binding energies of the $[BTTT]^+$–$[FeCl_4]^-$ and $[BTTT]^+$–$[BS]^-$ pairs, along with their difference ΔE_{ex}, decreased monotonically with increasing dielectric constant for all investigated solvents (Fig. 4b). The binding energy of the $[BTTT]^+$–$[FeCl_4]^-$ pair had the strongest correlation with the dielectric constant, even between **ACN** and **DMSO**, both of which exhibited similar binding energies for the $[BTTT]^+$–$[BS]^-$ pair and ΔE_{ex} values. In conjunction with a dramatic decrease in the electrical conductivity of the FeCl3-doped **PBTTT** film after **DBSA/DMSO** treatment compared to **DBSA/ACN** treatment, the DFT calculations suggest that the rapid dissociation of the $[FeCl_4]^-$ anion from the polaron in a polar solvent played a dominant role in causing
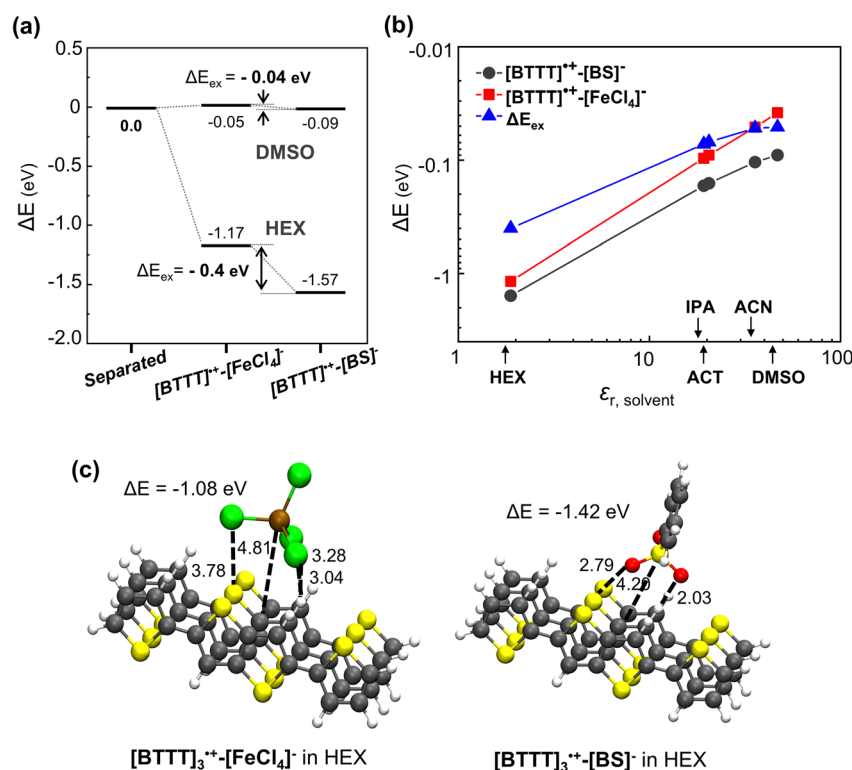
Fig. 4 Structures and energetics of polaron-dopant anion interactions calculated by density functional theory (DFT). (a) Energy diagram for the dopant ion exchange between $[BTTT]^+$–$[FeCl_4]^-$ and $[BTTT]^+$–$[BS]^-$ in hexane and **DMSO**. (b) Polaron-anion binding energies ($\Delta E([BTTT]^+$–$[BS]^-) - \Delta E([BTTT]^+$–$[FeCl_4]^-)$) for the stepwise doping processes with respect to the solvent's dielectric constant. (c) Optimized geometries and binding energies of π-stacked $[BTTT]_3^+$ paired with $[FeCl_4]^-$ (left) and $[BS]^-$ in **HEX** (right) in a front view. In panel (c), the dotted lines and numbers illustrate the interatomic distance in units of Å.

This journal is © The Royal Society of Chemistry 2025

J. Mater. Chem. A, 2025, **13**, 18966–18977 | **18973**

dedoping instead of anion exchange during the **DBSA** treatment.

The DFT-optimized geometries of the polaron-anion dimers revealed that, in all investigated solvents, both $[FeCl_4]^-$ and $[BS]^-$ anions preferentially bound to the side of the thieno-thiophene ring in $[BTTT]^+$ (Fig. 4c). Consequently, the two anions were expected to compete for binding to the same site on the $[BTTT]^+$ during the anion exchange, resulting in the replacement of the more weakly bound $[FeCl_4]^-$ anion. This dopant-ion binding motif predicted by our DFT model aligns with the results of an experimental study on $FeCl_3$-doped C12-**PBTTT**, where the dopant ionic species were observed to inter-calate into the space between the lamellae of a C12-**PBTTT** crystal. We note that the predicted orientation of anion binding did not interfere with the π–π stacking of **PBTTT** chains, and the relative binding strengths of the anions to polarons were consistent in DFT calculations considering either a single chain or three stacked chains of BTTT (Fig. S7†), as well as in auxiliary DFT calculations with extended BTTT trimer systems to elimi-nate the artifact caused by confining the polaron charge in

a monomer of BTTT (Fig. S8–S10†). The anion binding orien-tations and the exothermicity of ion exchange in the trimeric polaron systems were consistent with the results for the monomeric polaron systems, supporting the validity of the molecular physical arguments for the monomeric systems.

Finally, the anion exchange process was compared to direct doping. **DBSA** itself can generate charge carriers when added to **PBTTT** film. Although the mechanism of charge generation by **DBSA** has not been clearly elucidated, a recent report on the doping mechanism of poly[2,6-(4,4-bis(2-hexadecyl)-4H-cyclo-penta[2,1-b;3,4-b']dithiophene)-alt-4,7(2,1,3-benzothiadiazole)] (PCPDTBT) by the tris(pentafluoro-phenyl)borane–H_2O (BCF–H_2O) complex suggests that charge generation may occur *via* Brønsted-acid doping,[37] in which protonation oxidizes the conjugated polymer backbones. When a **PBTTT** film was doped by immersion in a **DBSA** solution with **HEX** as the solvent, the electrical conductivity of the **PBTTT** film gradually increased, reaching a value comparable to that achieved by $FeCl_3$ doping after an immersion time of 5 h (Fig. 5a). Such doping of conjugated polymers *via* direct protonation was unlikely to
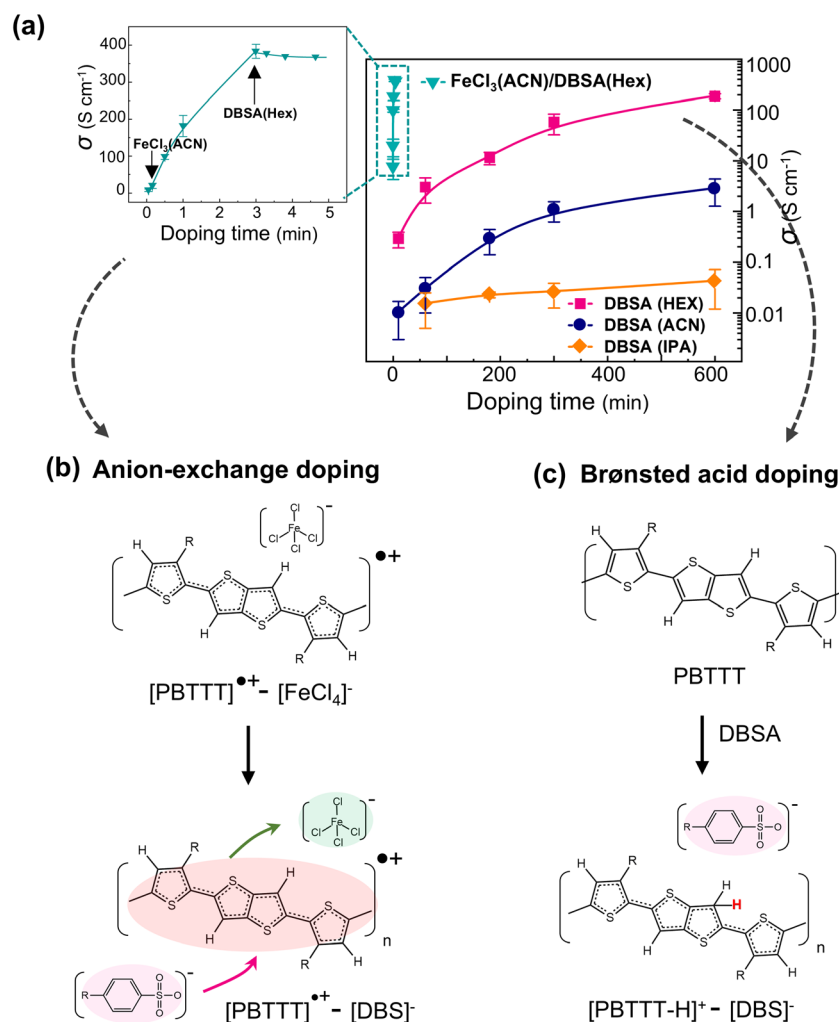

Fig. 5 (a) σ of $FeCl_3$(**ACN**)/**DBSA**(**HEX**)-doped and **DBSA**-doped **PBTTT** films with respect to the doping time. The inset is the magnification for σ of $FeCl_3$(**ACN**)/**DBSA**(**HEX**)-doped **PBTTT** films with a doping time < 5 min. Chemical processes of (b) anion-exchange doping and (c) direct Brønsted acid doping.

occur in doping *via* anion exchange, because the $[FeCl_4]^-$ anion would quickly react with the protonated conjugated polymer, forming $FeCl_3$ and HCl.[44] The very short time (<1 min) required for **DBSA** doping *via* anion exchange suggests that **PBTTT** underwent negligible protonation, which would otherwise require a much longer time (>1 h) to induce a noticeable enhancement in electrical conductivity.

The choice of solvent significantly affected both direct doping and anion exchange. The use of a non-polar solvent improved the electrical conductivity of **PBTTT** films doped by both anion exchange and direct doping. However, doping *via* anion exchange required an immersion time of less than 10 min for each dipping in $FeCl_3$ and **DBSA** solutions, whereas the direct doping by **DBSA** did not exhibit a plateau in the electrical conductivity after immersion in the **DBSA** solution for 5 h. Stepwise doping *via* anion exchange effectively shortened the overall processing time by using a strong redox agent ($FeCl_3$) to oxidize the conjugated polymer and form an intermediate ion-pair, where the anion was vulnerable to environmental factors. The subsequent exchange of this anion with a bulky ion formed a stable ion-pair with a strong binding state (Fig. 5b). In contrast, doping directly such a bulky ion *via* Brønsted-acid doping required a much longer time to oxidize the conjugated polymer due to its low redox potential (Fig. 5c). Interestingly, the best solvent to achieve a high electrical conductivity varied for each step: $FeCl_3$ doping was most effective with a partially polar solvent (**ACN**), while anion exchange with **DBSA** was favored with a non-polar solvent (**HEX**). The model study using **DBSA** emphasizes the importance of choosing the proper solvent, potentially opening new possibilities of achieving both high doping levels and a stable doped state in organic semiconductors.

3. Conclusion

We demonstrated sequential ion-exchange doping of **PBTTT** film using $FeCl_3$ and a Brønsted acid, **DBSA**, in solvents with various dielectric constants. The molecular mechanism involved several stages, including the diffusion of the second anion solution into the crystal interlayer space of the **PBTTT** film, the replacement of $[FeCl_4]^-$ with $[DBS]^-$ at the polaron sites, and the long-term stabilization of the polaron-dopant pair after completion of anion exchange. The final doping level achieved by ion exchange depended on the ability of the solvent to preserve the polaron-dopant pairs without causing polaron annihilation and on the thermodynamic spontaneity of the ion replacement process at polaron sites. Using a solvent with a low dielectric constant for the second anion solution resulted in a high electrical conductivity due to the following factors throughout the process: (i) enhanced access of the second anion to polaron sites, originating from good anion solubility and CP miscibility, and (ii) improved rate of anion exchange under non-polar conditions. Replacing $[FeCl_4]^-$ with $[DBS]^-$ in a non-polar solvent improved the environmental stability of the doped **PBTTT** film under ambient conditions, preserving the high carrier density achieved by $FeCl_3$ doping. Additionally, **DBSA** required a long time to achieve high electrical conductivity

through direct doping as a Brønsted acid, whereas rapid ion exchange between $[DBS]^-$ and $[FeCl_4]^-$ achieved comparably high electrical conductivity in a very short time. We believe that this work deepens the understanding of the interactions among counter-ions, CPs, and solvent environments during ion-exchange doping of CP and contributes to the advancement of highly conductive organic semiconductors.

4. Experimental

FeCl₃/DBSA doped PBTTT film preparation

PBTTT (M_w > 50 kDa), $FeCl_3 \cdot 6H_2O$, **DBSA**, and all used solvents were purchased from Sigma-Aldrich. 0.5 wt% **PBTTT** solution was prepared by dissolving **PBTTT** powder in a mixed solvent (dichlorobenzene : cholorobenzene = 1 : 1). The solution was stirred for more than 3 h at 120 °C, and then was spun coated onto glass substrates at 1000 rpm for 30 s at room temperature. After that, **PBTTT** films were thermally annealed at 150 °C for 25 min to increase the crystallinity. 0.1 mM $FeCl_3 \cdot 6H_2O$ solution was prepared by dissolving $FeCl_3$ powder in acetonitrile. **PBTTT** films were immersed in $FeCl_3$ solution with the desired doping time, then blown out with N_2. Next, highly $FeCl_3$-doped **PBTTT** films were dipped in 0.1 mM **DBSA** solution for a desired period of time. The film was washed with solvent to remove the remaining **DBSA**. For Brønsted acid doping, undoped **PBTTT** film was directly dipped into 0.1 mM **DBSA** solution.

Contact angle measurement

The contact angle was measured by using a SmartDrop_Plus (Femtobiomed Inc.).[45] 20 μL of solvent droplet was controlled, then dropped onto the undoped **PBTTT** film.

Measurement of electrical properties

σ was obtained by using a four-point probe measurement system (MSTECH) and AFM.[46] The thickness of the undoped **PBTTT** film was about 25 nm, and it increased to 40 nm after doping.

Four-point probe FET methods

An FET device with bottom-gate, bottom-contact structure was prepared. 5/50 nm of Ti/Au electrodes were thermal evaporated on SiO_2 1000 nm/Si substrates. After that, the substrates were ODTS-treated in 0.5 vol% ODTS diluted in toluene. The active layer was prepared as described in the film preparation part. The electrical properties of OFETs were measured by using Keithley 2400 and 6514 source/measure units in the probe station under vacuum conditions.

Computational details

Computational details are provided in ESI Section 2.†

Data availability

The datasets used and/or analysed during the current study are available from the corresponding author on reasonable request.

This journal is © The Royal Society of Chemistry 2025

J. Mater. Chem. A, 2025, **13**, 18966–18977 | **18975**

Conflicts of interest

The authors declare no conflict of interest.

Acknowledgements

References

1 B. Russ, A. Glaudell, J. J. Urban, M. L. Chabinyc and R. A. Segalman, *Nat. Rev. Mater.*, 2016, **1**, 1–14.

2 O. Bubnova and X. Crispin, *Energy Environ. Sci.*, 2012, **5**, 9345–9362.

3 C. G. Shuttle, R. Hamilton, J. Nelson, B. C. O'Regan and J. R. Durrant, *Adv. Funct. Mater.*, 2010, **20**, 698–702.

4 I. Salzmann and G. Heimel, *J. Electron Spectrosc. Relat. Phenom.*, 2015, **204**, 208–222.

5 I. E. Jacobs and A. J. Moulé, *Adv. Mater.*, 2017, **29**, 1703063.

6 S. H. Kim, H. Yook, W. Sung, J. Choi, H. Lim, S. Chung, J. W. Han and K. Cho, *Adv. Mater.*, 2023, **35**, 2207320.

7 A. M. Glaudell, J. E. Cochran, S. N. Patel and M. L. Chabinyc, *Adv. Energy Mater.*, 2015, **5**, 1401072.

8 W. Zhao, J. Ding, Y. Zou, C.-a. Di and D. Zhu, *Chem. Soc. Rev.*, 2020, **49**, 7210–7228.

9 I. Salzmann, G. Heimel, M. Oehzelt, S. Winkler and N. Koch, *Acc. Chem. Res.*, 2016, **49**, 370–378.

10 Y. Liu, B. Nell, K. Ortstein, Z. Wu, Y. Karpov, T. Beryozkina, S. Lenk, A. Kiriy, K. Leo and S. Reineke, *ACS Appl. Mater. Interfaces*, 2019, **11**, 11660–11666.

11 Y. Karpov, T. Erdmann, I. Raguzin, M. Al-Hussein, M. Binner, U. Lappan, M. Stamm, K. L. Gerasimov, T. Beryozkina and V. Bakulev, *Adv. Mater.*, 2016, **28**, 6003–6010.

12 K. Kang, S. Watanabe, K. Broch, A. Sepe, A. Brown, I. Nasrallah, M. Nikolka, Z. Fei, M. Heeney and D. Matsumoto, *Nat. Mater.*, 2016, **15**, 896–902.

13 J. Min, J. Im, S. H. Kim, H. H. Choi and K. Cho, *Adv. Funct. Mater.*, 2023, **33**, 2212825.

14 J. Min, D. Kim, S. G. Han, C. Park, H. Lim, W. Sung and K. Cho, *Adv. Electron. Mater.*, 2022, **8**, 2101142.

15 Y. W. Park, A. J. Heeger, M. A. Druy and A. G. MacDiarmid, *J. Chem. Phys.*, 1980, **73**, 946–957.

16 K. Walzer, B. Maennig, M. Pfeiffer and K. Leo, *Chem. Rev.*, 2007, **107**, 1233–1271.

17 V. Vijayakumar, Y. Zhong, V. Untilova, M. Bahri, L. Herrmann, L. Biniek, N. Leclerc and M. Brinkmann, *Adv. Energy Mater.*, 2019, **9**, 1900266.

18 N.-H. Park, E. S. Shin, G.-S. Ryu, J. Kwon, D. Ji, H. Park, Y. H. Kim and Y.-Y. Noh, *J. Inf. Disp.*, 2022, **24**, 109–118.

19 I. E. Jacobs, E. W. Aasen, J. L. Oliveira, T. N. Fonseca, J. D. Roehling, J. Li, G. Zhang, M. P. Augustine, M. Mascal and A. J. Moulé, *J. Mater. Chem. C*, 2016, **4**, 3454–3466.

20 E. Lim, K. A. Peterson, G. M. Su and M. L. Chabinyc, *Chem. Mater.*, 2018, **30**, 998–1010.

21 H. Tang, Y. Liang, C. Liu, Z. Hu, Y. Deng, H. Guo, Z. Yu, A. Song, H. Zhao, D. Zhao, Y. Zhang, X. Guo, J. Pei, Y. Ma, Y. Cao and F. Huang, *Nature*, 2022, **611**, 271–277.

22 I. E. Jacobs, Y. Lin, Y. Huang, X. Ren, D. Simatos, C. Chen, D. Tjhe, M. Statz, L. Lai, P. A. Finn, W. G. Neal, G. D'Avino, V. Lemaur, S. Fratini, D. Beljonne, J. Strzalka, C. B. Nielsen, S. Barlow, S. R. Marder, I. McCulloch and H. Sirringhaus, *Adv. Mater.*, 2022, **34**, 2102988.

23 Y. Yamashita, J. Tsurumi, M. Ohno, R. Fujimoto, S. Kumagai, T. Kurosawa, T. Okamoto, J. Takeya and S. Watanabe, *Nature*, 2019, **572**, 634–638.

24 C. Zhong, Y. Deng, W. Hu, J. Qiao, L. Zhang and J. Zhang, *Chem. Soc. Rev.*, 2015, **44**, 7484–7539.

25 C. Moreau and G. Douhéret, *J. Chem. Thermodyn.*, 1976, **8**, 403–410.

26 S. N. Patel, A. M. Glaudell, K. A. Peterson, E. M. Thomas, K. A. O'Hara, E. Lim and M. L. Chabinyc, *Sci. Adv.*, 2017, **3**, e1700434.

27 O. Zapata-Arteaga, A. Perevedentsev, M. Prete, S. Busato, P. S. Floris, J. Asatryan, R. Rurali, J. Martin and M. Campoy-Quiles, *ACS Energy Lett.*, 2024, **9**, 3567–3577.

28 C. V. Krishnan and H. L. Friedman, *J. Phys. Chem.*, 1971, **75**, 3598–3606.

29 S. E. Yoon, J. M. Han, B. E. Seo, S.-W. Kim, O.-P. Kwon, B.-G. Kim and J. H. Kim, *Org. Electron.*, 2021, **90**, 106061.

30 I. McCulloch, M. Heeney, C. Bailey, K. Genevicius, I. MacDonald, M. Shkunov, D. Sparrowe, S. Tierney, R. Wagner and W. Zhang, *Nat. Mater.*, 2006, **5**, 328–333.

31 T. Ma, B. X. Dong, G. L. Grocke, J. Strzalka and S. N. Patel, *Macromolecules*, 2020, **53**, 2882–2892.

32 H. Tanaka, K. Kanahashi, N. Takekoshi, H. Mada, H. Ito, Y. Shimoi, H. Ohta and T. Takenobu, *Sci. Adv.*, 2020, **6**, eaay8065.

33 Y. Kim, S. Chung, K. Cho, D. Harkin, W. T. Hwang, D. Yoo, J. K. Kim, W. Lee, Y. Song and H. Ahn, *Adv. Mater.*, 2019, **31**, 1806697.

34 N. A. Mustaffa, Q. Ahsan, M. A. Azam and L. C. Abdullah, *Malays. J. Anal. Sci.*, 2017, **21**, 950–957.

35 J. E. Cochran, M. J. Junk, A. M. Glaudell, P. L. Miller, J. S. Cowart, M. F. Toney, C. J. Hawker, B. F. Chmelka and M. L. Chabinyc, *Macromolecules*, 2014, **47**, 6836–6846.

36 Y. Yamashita, J. Tsurumi, T. Kurosawa, K. Ueji, Y. Tsuneda, S. Kohno, H. Kempe, S. Kumagai, T. Okamoto, J. Takeya and S. Watanabe, *Commun. Mater.*, 2021, **2**, 45.

37 B. Yurash, D. X. Cao, V. V. Brus, D. Leifert, M. Wang, A. Dixon, M. Seifrid, A. E. Mansour, D. Lungwitz and T. Liu, *Nat. Mater.*, 2019, **18**, 1327–1334.

38 E. Alveroglu, *J. Mol. Struct.*, 2015, **1086**, 86–92.

39 J. Fraxedas, A. Vollmer, N. Koch, D. de Caro, K. Jacob, C. Faulmann and L. Valade, *Materials*, 2021, **14**, 2058.

40 P. Kappen, N. Brack, P. S. Hale, W. Prissanaroon, E. Welter and P. J. Pigram, *Appl. Surf. Sci.*, 2005, **243**, 287–295.

41 H. H. Choi, Y. I. Rodionov, A. F. Paterson, J. Panidi, D. Saranin, N. Kharlamov, S. I. Didenko,

18976 | *J. Mater. Chem. A*, 2025, **13**, 18966–18977

This journal is © The Royal Society of Chemistry 2025

T. D. Anthopoulos, K. Cho and V. Podzorov, *Adv. Funct. Mater.*, 2018, **28**, 1707105.

42 K. Kang, S. Schott, D. Venkateshvaran, K. Broch, G. Schweicher, D. Harkin, C. Jellett, C. B. Nielsen, I. McCulloch and H. Sirringhaus, *Mater. Today Phys.*, 2019, **8**, 112–122.

43 E. M. Thomas, K. A. Peterson, A. H. Balzer, D. Rawlings, N. Stingelin, R. A. Segalman and M. L. Chabinyc, *Adv. Electron. Mater.*, 2020, **6**, 2000595.

44 P. Taylor, *Electrophilic Aromatic Substitution Reactions*, The Open University, UK, 2002.

45 J. Son, G. Y. Bae, S. Lee, G. Lee, S. W. Kim, D. Kim, S. Chung and K. Cho, *Adv. Mater.*, 2021, **33**, 2102740.

46 D. Kim, D. Ju and K. Cho, *Adv. Mater. Technol.*, 2018, **3**, 1700335.

This journal is © The Royal Society of Chemistry 2025

J. Mater. Chem. A, 2025, **13**, 18966–18977 | **18977**